IEEE Access
Multidisciplinary | Rapid Review | Open Access Journal

Received October 11, 2021, accepted November 3, 2021, date of publication December 1, 2021, date of current version January 10, 2022.

*Digital Object Identifier 10.1109/ACCESS.2021.3132280*

# Influence of Complex Fluid Flow on Temperature Distribution in the Rotor Region of Large Hydrogenerator Under the Rotor Rotation

**HAN JICHAO[1,2,3,4], SUN YUTIAN[1,2,3], ZHENG PING[5], QI HAIMING[4], DONG JIECHEN[4], LIU YUFEI[4], ZHANG CHUNLI[3], GE BAOJUN[4], AND LI WEILI[4]**

[1]State Key Laboratory of Hydro-power Equipment, Harbin 150040, China
[2]Harbin Electric Machinery Company Ltd., Harbin 150040, China
[3]Harbin Institute of Large Electrical Machinery, Harbin 150040, China
[4]School of Electrical and Electronic Engineering, Harbin University of Science and Technology, Harbin 150080, China
[5]Harbin Institute of Technology, Harbin 150001, China

Corresponding author: Han Jichao (hanjichao163@163.com)

This work was supported in part by the National Natural Science Foundation of China under Grant 52177037, in part by the National Natural Science Foundation of China under Grant 51807043, in part by the Natural Science Foundation of Heilongjiang Province of China under Grant YQ2021E037, in part by the Research Foundation of State Key Laboratory of Hydro-Power Equipment under Grant SKLHE-ORF-202001, in part by the Fundamental Research Foundation for Universities of Heilongjiang Province under Grant 2019-KYYWF-0209, in part by the Postdoctoral Foundation of Heilongjiang Province of China under Grant LBH-TZ1005, in part by the China Postdoctoral Science Foundation under Grant 2018T110269, in part by the China Postdoctoral Science Foundation under Grant 2018M630336, in part by the Postdoctoral Foundation of Heilongjiang Province of China under Grant LBH-Z17040, and in part by the Fundamental Research Foundation for Universities of Heilongjiang Province under Grant 2018-KYYWF-1629.

**ABSTRACT** Ventilation cooling design is one of the key technologies during the design of large hydrogenerator. With the increase of hydrogenerator capacity, the overheating problem of rotor region become more and more serious. In this paper, a 250 MW hydrogenerator is analyzed. The transient electromagnetic field of the hydrogenerator is calculated. The losses (heat sources) of rotor components in the rotor region of the hydrogenerator are determined. Three-dimensional fluid and thermal coupled mathematic model of the hydrogenerator rotor region is established. The rotor rotation of the hydrogenerator is considered. The distribution of complex fluid velocity in the rotor region is calculated using the finite volume method. The influence of fluid velocity in the different directions on the temperature of the rotor excitation winding is studied under the different flow rates in the rotor region. The surface heat-transfer coefficient distribution of the rotor components is determined. The temperature distribution of the rotor excitation winding, rotor pole body, rotor press plate, rotor damping bar, and rotor end ring is obtained. The calculated temperature results match well with test values. These provide an important reference for the rotor structural design and optimization of larger hydrogenerator.

**INDEX TERMS** Hydrogenerator, electromagnetic field, rotor rotation, fluid velocity, different directions, temperature distribution.

## I. INTRODUCTION

Hydroelectric power generation is one of the cleanest methods of power generation. Hydrogenerator is the core equipment in the entire hydropower system, which plays a vital role. With the rapid development of hydroelectric power generation technology, the capacity of hydrogenerator continues to increase. The efficiency of hydrogenerator and the utilization of materials improve obviously. However, as the capacity of hydrogenerator increases, the overheating problem of hydrogenerator rotor region becomes more and more serious. It has seriously threatened the stability, safe operation, and service life of hydrogenerator. Furthermore, the heat of the rotor components is taken away by the complex fluid flow in the rotor region. Therefore, a study of influence of complex fluid flow on temperature distribution in the rotor region of large hydrogenerator is of great significance when the rotor rotation is considered.

In recent years, numerous studies researched on the physical field in the large generator. For example,

The associate editor coordinating the review of this manuscript and approving it for publication was Su Yan.

C. Carounagarane *et al* studied the temperature distribution of the hydrogenerator under 10% and 20% continuous overloads through the coupling thermal and fluid-dynamical analysis [1]. H. C. Dirani *et al* studied the impact of rotor interturn short circuit on radial flux density, radial force density, unbalanced magnetic pull, and electromagnetic torque of a 74-MVA industrial large hydrogenerator with 76 poles [2]. G. Traxler-Samek *et al* describes an analytical algorithm for the calculation of currents and corresponding losses in the damper winding [3]. M. Ranlöf *et al* proposed a permeance model that can be employed to estimate the no-load damper current loss and voltage waveform harmonics in large hydrogenerators [4]. A. Z. Gbégbé *et al* studied a large hydrogenerator modeling method that provides an excellent compromise between accuracy and speed [5]. S. E. Dallas *et al* presents an investigation of the behavior of a 200-MVA-synchronous hydrogenerator during interturn stator fault. It focuses on the affection to the electromagnetic magnitudes, such as the currents and the electromagnetic torque [6]. J. C. Akiror *et al* studied rotational flux distribution in the stator of the hydrogenerator under different operating conditions [7]. T. Øyvang *et al* proposed and verified an air-cooled hydrogenerators heating network for real-time monitoring and optimal control [8]. S. Li *et al* studied the flux and loss distributions in the end region of large generators by transient 3-dimensional finite-element method. The in-plate loss contribution from the flux in the Z direction on the out most several packets of the stator laminations is considered. Parametric study is carried out to evaluate the effectiveness of various candidate designs in reducing the losses in the end region of large generators [9]–[13]. Some other experts extensively studied hydrogenerator [14], [15], but very few focused on the influence of complex fluid flow on temperature distribution in the rotor region of large hydrogenerator under the rotor rotation.

This paper is the continuation of the reference [16]. In reference [16], it focused on the influence of different rotor structures on the temperature distribution in the rotor region of hydrogenerator. However, this paper focuses on the influence of fluid velocity in the different directions on the temperature distribution of the rotor components under the different flow rates in the rotor region of hydrogenerator. In this paper, a 250 MW hydrogenerator is analyzed. The transient electromagnetic field of the hydrogenerator is established. The losses (heat sources) of rotor components in the rotor region of the hydrogenerator are determined. Three-dimensional fluid and thermal coupled mathematic model of the hydrogenerator rotor region is established. The rotor rotation of the hydrogenerator is considered. The distribution of complex fluid velocity in the rotor region is calculated using the finite volume method. The influence of fluid velocity in the different directions on the temperature of the rotor excitation winding is studied in detail under the different flow rates in the rotor region. The surface heat-transfer coefficient distribution of the rotor components is determined. The temperature distribution of the rotor excitation winding, rotor pole body, rotor press plate, rotor damping bar, and rotor end ring is obtained. It provides an important reference for the rotor structural design of larger hydrogenerator.

## II. ESTABLISHMENT OF TWO-DIMENSIONAL TRANSIENT ELECTROMAGNETIC FIELD MODEL OF HYDROGENERATOR

Fig. 1 gives this 250MW hydrogenerator unit. Fig. 1(a) shows the hydrogenerator unit. Fig. 1(b) shows the hydrogenerator rotor. According to the actual structure of the 250MW hydrogenerator, the mathematical model of two-dimensional transient electromagnetic field is established in the 250MW hydrogenerator [17]. Fig. 2 gives the solved region of the two-dimensional transient electromagnetic field of the hydrogenerator. Fig. 3 shows the meshing map. Table 1 shows the basic parameters of this hydrogenerator.

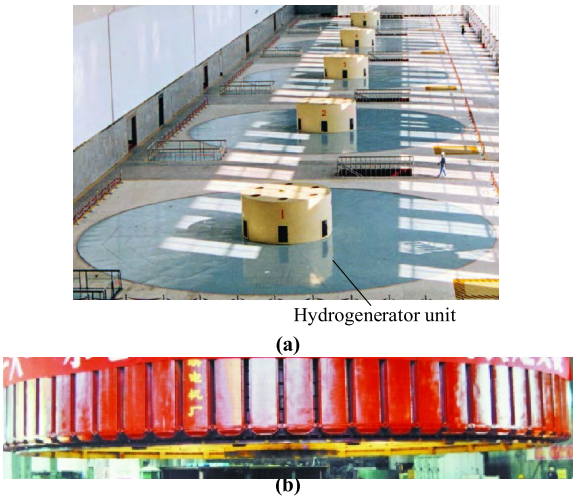


**FIGURE 1.** 250MW hydrogenerator unit. a) Hydrogenerator unit. b) Hydrogenerator rotor.

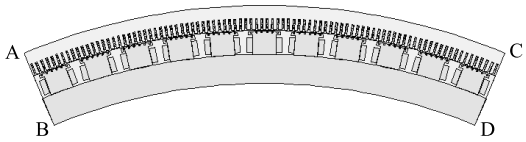


**FIGURE 2.** Solved region of the two-dimensional transient electromagnetic field of the hydrogenerator.

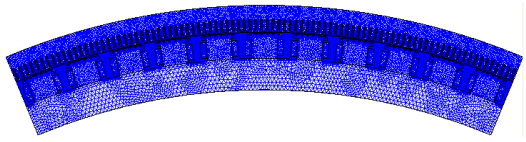

**FIGURE 3.** Meshing map.

Fig. 4 shows flux distribution at the axial middle position of the hydrogenerator. The loss of the rotor magnetic pole surface is caused by the tooth harmonic magnetic field.

**TABLE 1. Basic parameters of this hydrogenerator.**

| | | | |
|---|---|---|---|
| Rated power (MW) | 250 | Number of poles | 88 |
| Rated speed (r/min) | 68.2 | Frequency (Hz) | 50 |
| Inner diameter of stator (mm) | 16620 | Outer diameter of rotor (mm) | 16580 |

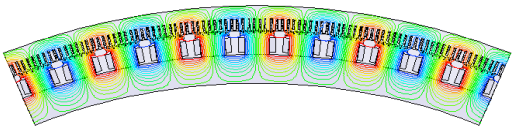

**FIGURE 4. Flux distribution of this hydrogenerator.**

It includes: (1) Rotor surface loss $P_{kv}$ caused by the stator windings MMF harmonic. (2) Additional loss $P_{\mathrm{Fe}P}$ of the rotor magnetic pole surface under no-load rated voltage. (3) Additional loss $P_{2vk}$ caused by harmonic MMF of stator teeth on the surfaces of the rotor magnetic pole and rotor damper bar. The loss of the rotor exciting winding is 558.1 kW. Table 2 shows the additional loss of the rotor magnetic pole surface.

**TABLE 2. Addition loss of the rotor magnetic pole surface.**

| | $P_{kv}$(kW) | $P_{\mathrm{Fe}P}$(kW) | $P_{2vk}$(kW) |
|---|---|---|---|
| Design values | — | 194.05 | 42.535 |
| Calculated results | 9.13 | 190.75 | 44.78 |

## III. ESTABLISHMENT OF THREE-DIMENSIONAL FLUID AND THERMAL COUPLED MATHEMATIC MODEL OF HYDROGENERATOR

Fig. 5 shows the ventilation system of this hydrogenerator. It includes the stator core, stator winding, rotor exciting winding, rotor yoke ventilation duct, magnet yoke, rotor support, wind plate, cooler, etc. According to the actual structure of the hydrogenerator rotor region, three-dimensional fluid and thermal coupled model of rotor region is established, as shown in Fig. 6. Fig. 6(a) shows the solving region of hydrogenerator rotor. Fig. 6(b) gives the rotor components. It includes mainly the rotor excitation winding, rotor magnetic yoke, rotor support plate, rotor pole body, rotor damper bar, rotor end ring, rotor press plate, and rotor pole body insulation, etc. In Fig. 6(a), x direction represents the circumferential direction of the hydrogenerator, y direction represents the radial direction of the hydrogenerator, and z direction represents the axial direction of the hydrogenerator. Cold air from cooler enters into the inlet of the rotor region. After cooling the rotor components, the hot air flows out from the outlet of the rotor region. The rotation speed of the hydrogenerator rotor is 68.2r/min. The fluid temperature of the rotor region inlet is 40°C under the rated load condition.

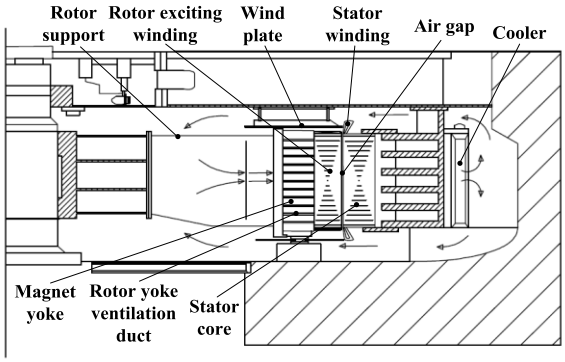


**FIGURE 5. Ventilation system of air-cooled hydrogenerator.**

In the hydrogenerator rotor region, the equations for the 3-D fluid and thermal coupled analysis model in the hydrogenerator rotor region are given as follows [18]–[21]:

$$\begin{cases} \dfrac{\partial \rho}{\partial t} + \nabla \cdot (\rho \vec{v}) = 0 \\ \dfrac{\partial}{\partial t}(\rho \vec{v}) + \nabla \cdot (\rho \vec{v}\vec{v}) = -\nabla p + \nabla \cdot (\bar{\bar{\tau}}) + \rho \vec{g} + \vec{F} \\ \dfrac{\partial}{\partial t}(\rho E) + \nabla \cdot (\vec{v}(\rho E + p)) = \nabla \cdot (k_{eff} \nabla T \\ \qquad - \sum_j h_j \vec{J}_j + (\bar{\bar{\tau}}_{eff} \cdot \vec{v})) + S_h \\ \dfrac{\partial}{\partial t}(\rho k) + div(\rho k \mathbf{u}) = div\left[\left(\mu + \dfrac{\mu_t}{\sigma_k}\right) grad k\right] + G_k - \rho\varepsilon \\ \dfrac{\partial}{\partial t}(\rho \varepsilon) + div(\rho \mathbf{u} \varepsilon) = div\left[\left(\mu + \dfrac{\mu_t}{\sigma_\varepsilon}\right) grad \varepsilon\right] + G_{1\varepsilon}\dfrac{\varepsilon}{k} G_k \\ -G_{2\varepsilon}\rho\dfrac{\varepsilon^2}{k} \end{cases} \tag{1}$$

where $\vec{v}$ is velocity vector, $\rho$ is fluid density, $t$ is time, $p$ is static pressure, $\rho\vec{g}$ and $\vec{F}$ are gravitational body force and external body forces, $\bar{\bar{\tau}}$ is stress tensor, $I$ is the unit tensor, $\mu$ is the molecular viscosity, $\vec{J}_j$ is the diffusion flux of species $j$, $S_h$ includes the heat of chemical reaction and any other volumetric heat sources, $k$ is kinetic energy of turbulence, $\mu_t$ is the turbulent viscosity coefficient, $k_{eff}$ is the effective conductivity, $G_k$ is the generation rate of the turbulence, $\varepsilon$ is diffusion factor, $\sigma_k$ and $\sigma_\varepsilon$ are Planck constants, $G_{1\varepsilon}$ and $G_{2\varepsilon}$ are constants.

## IV. 3-D FLUID AND THERMAL COUPLED ANALYSIS MODEL IN THE HYDROGENERATOR ROTOR REGION

This paper focuses on the loss of rotor magnetic pole surface, the loss of rotor exciting winding, complex fluid velocity, and temperature distribution of rotor components in the rotor region of large hydrogenerator. When the problems of fluid flow and heat transfer are solved, the finite element method is not as mature as the finite volume method in terms of the discrete processing method of convection term and the

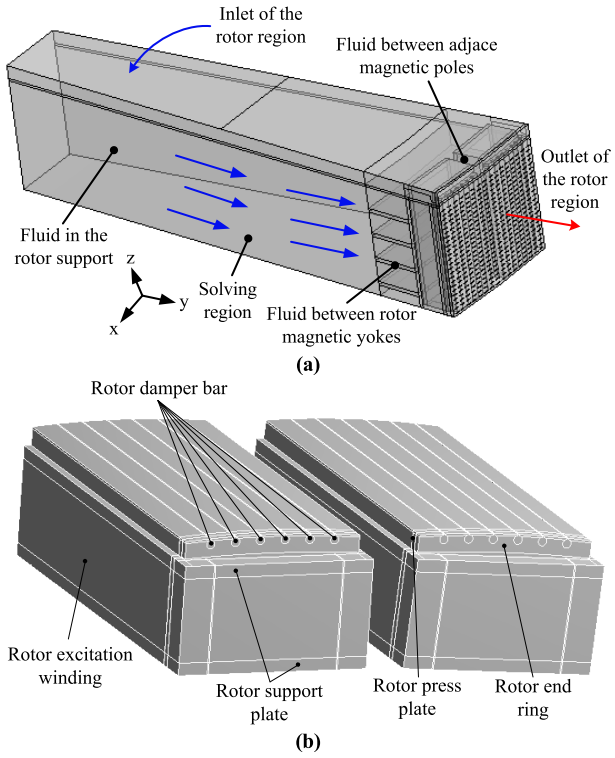


**FIGURE 6.** Three-dimensional fluid and thermal coupled model of hydrogenerator rotor region. a) Solving region of hydrogenerator rotor. b) Rotor components.

original variable solution method of incompressible fluid. The complex fluid velocity and the temperature distribution of rotor components are calculated using the finite volume method in this paper. In the 3-D fluid and thermal coupled analysis model in the rotor region of hydrogenerator, the loss values from electromagnetic field calculation are applied to the rotor components as heat sources in the temperature field. The rotor rotation of the hydrogenerator is considered. After solving the fluid and thermal equations of fluid-solid conjugated heat transfer, fluid velocity and temperature distribution are obtained in the rotor region of hydrogenerator [22]–[27]. The influence of fluid velocity in the different directions on the temperature of the rotor excitation winding is studied under the different flow rates in the hydrogenerator rotor region.

### *A. DISTRIBUTION OF FLUID VELOCITY IN THE DIFFERENT DIRECTIONS BETWEEN ROTOR MAGNETIC POLES*

Fig. 7 shows the distribution of fluid velocity in the rotor region of hydrogenerator.

In Fig. 7, the highest fluid velocity is 80m/s and it appears in the outlet of the rotor region. The highest temperature of the hydrogenerator rotor region appears in the rotor excitation winding. The fluid velocity between the rotor magnetic poles affects directly the temperature distribution of the rotor excitation winding. When the hydrogenerator rotor rotates, the distribution of fluid velocity between the rotor magnetic poles is very complicated. In order to study the influence of

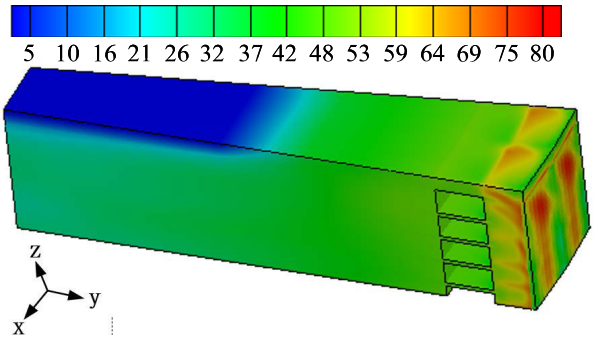


**FIGURE 7.** Distribution of fluid velocity in the rotor region of hydrogenerator.

fluid velocity in the different directions on the temperature of the rotor excitation winding, three sample lines are selected between the rotor magnetic poles, respectively. Three black sample lines A, B, C locate around the leeward side of the rotor excitation winding. Three red sample lines D, E, F locate around the windward side of the rotor excitation winding, as shown in Fig. 8. The synthetic fluid velocity and the fluid velocity in different directions on these sample lines are obtained when the fluid velocity of rotor region inlet is v1 = 2.5m/s, v2 = 2m/s, and v3 = 1.5m/s, respectively. The influence of fluid velocity in different directions on the temperature of the rotor excitation winding is studied in detail.

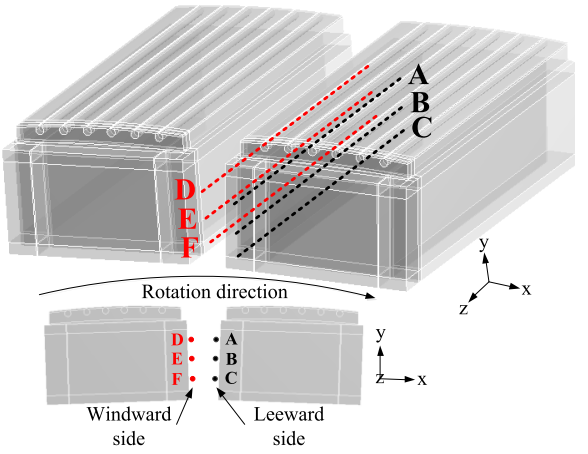


**FIGURE 8.** Lactation of sample lines around the windward side and the leeward side of the rotor excitation winding.

Fig. 9 shows the distribution of synthetic fluid velocity around the leeward side of the rotor excitation winding. Fig. 10 shows the distribution of synthetic fluid velocity around the leeward side of the rotor excitation winding.

In Fig. 9 and Fig. 10, fluid velocity fluctuates up and down along the axial direction. Since cooling fluid flows out from the rotor yoke ventilation duct, it results in a higher fluid velocity around the outlet of the rotor yoke ventilation duct. The fluid velocity is also relatively high near the rotor end region. As the fluid rate of rotor region inlet increases, the

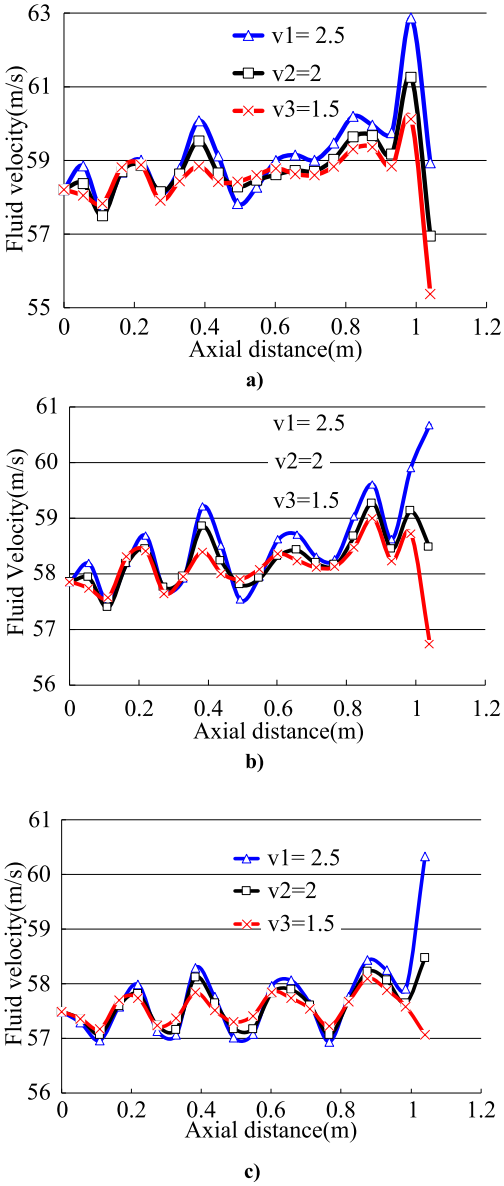


**FIGURE 9.** Distribution of synthetic fluid velocity around the leeward side of the rotor excitation winding. a) Sample line A. b) Sample line B. c) Sample line C.

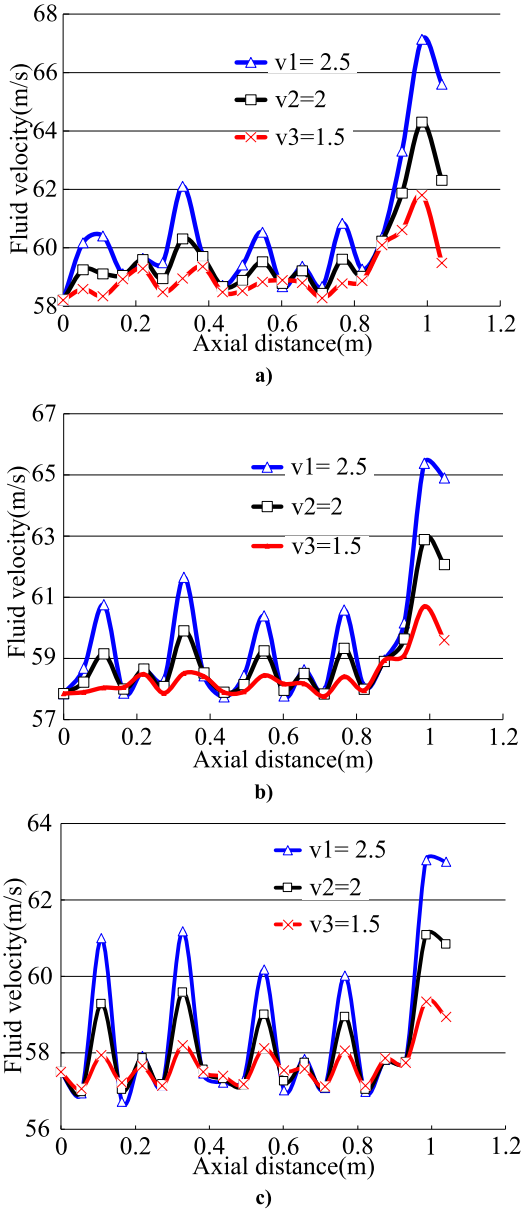


**FIGURE 10.** Distribution of synthetic fluid velocity around the windward side of the rotor excitation winding. a) Sample line D. b) Sample line E. c) Sample line F.

fluid velocity around the leeward side and windward side of the rotor excitation winding increase accordingly at the same position. When the hydrogenerator rotor rotates, the fluid velocity around the windward side of the rotor excitation winding changes obviously along the axial direction.

The temperature of the rotor excitation winding is relatively high in the rotor region of the hydrogenerator. In order to study the contribution of fluid velocity in the radial direction, circumferential direction, and axial direction to the cooling of the rotor excitation winding, Fig. 11-Fig. 16 give the distribution of fluid velocity in the radial direction, circumferential direction, and axial direction around the windward side and leeward side of the rotor excitation winding. Fig. 11 and Fig. 12 show the distribution of fluid velocity in the circumferential direction around the leeward side and windward side of the rotor excitation winding. The rotor rotation direction is clockwise and fluid velocity in the circumferential direction is negative. The distribution of the fluid velocity in the circumferential direction is basically the same along the axial direction under the different flow rates. The rotor rotation drives the fluid flow in a circumferential direction. The change of the fluid velocity of rotor region inlet has little effect on fluid velocity in the circumferential direction. There is a certain difference of fluid velocity in the circumferential direction around the windward side and the leeward side of

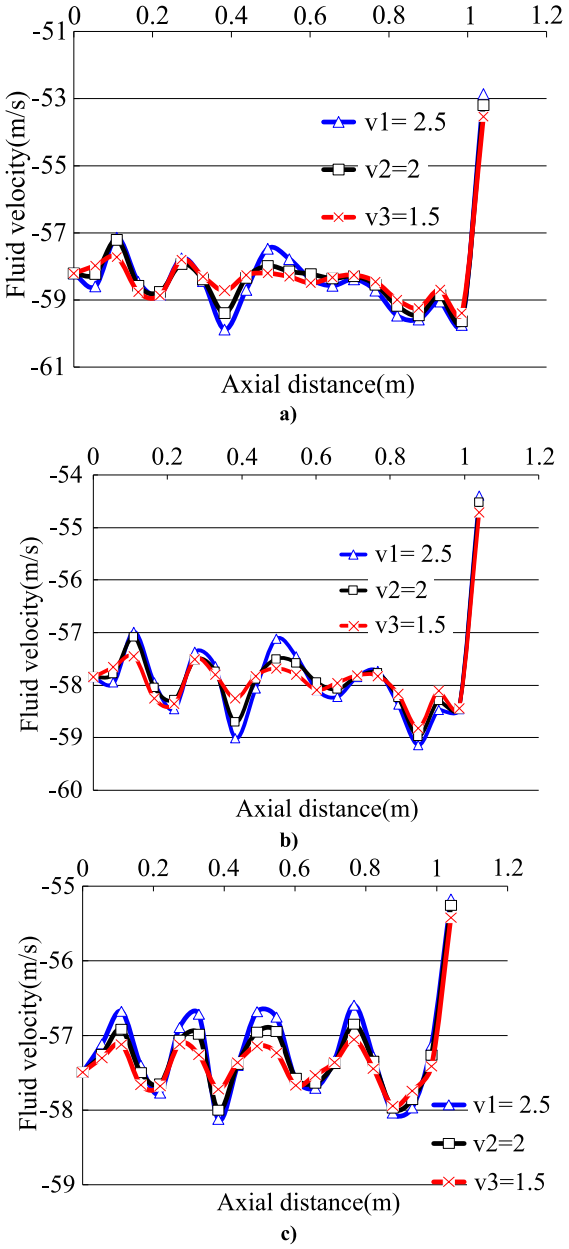


**FIGURE 11.** Distribution of fluid velocity in the circumferential direction around the leeward side of the rotor excitation winding. a) Sample line A. b) Sample line B. c) Sample line C.

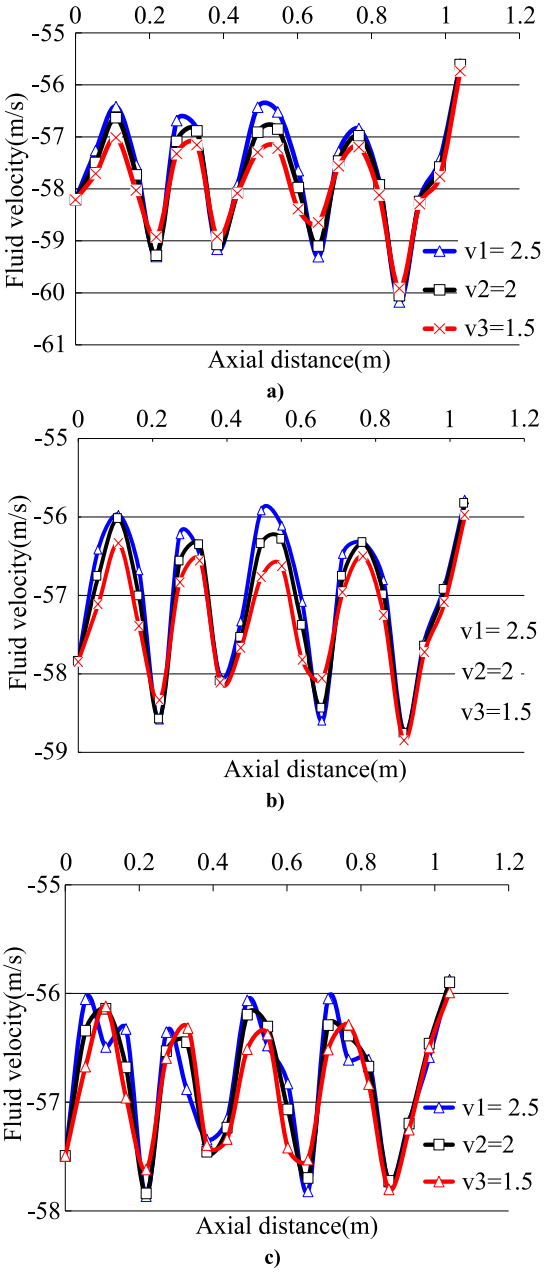


**FIGURE 12.** Distribution of fluid velocity in the circumferential direction around the windward side of the rotor excitation winding. a) Sample line D. b) Sample line E. c) Sample line F.

the rotor excitation winding. The fluid velocity in the circumferential direction fluctuates obviously around the windward side of the rotor excitation winding, while the fluid velocity in the circumferential direction is relatively stable around the leeward side of the rotor excitation winding along the axial direction within the range of 0m∼0.98m. The fluid velocity in the circumferential direction drops obviously near the rotor end region.

Fig. 13 and Fig. 14 show the distribution of fluid velocity in the radial direction around the leeward side and windward side of the rotor excitation winding. When the fluid velocity of rotor region inlet changes, the distribution of the fluid velocity in the radial direction is basically the same around the leeward side of the rotor excitation winding along the axial direction within the range of 0m∼0.98m. The fluid velocity is low and negative along the axial direction within the range of 0m∼0.98m. It shows that the fluid velocity reverses around the leeward side. The maximum fluid velocity in the radial direction is −5m/s. The fluid velocity in the radial direction increases obviously in the rotor end region. The fluid velocity fluctuates obviously around the windward side of the rotor excitation winding. Most fluid velocities in the radial direction are positive. The highest fluid velocity in the radial

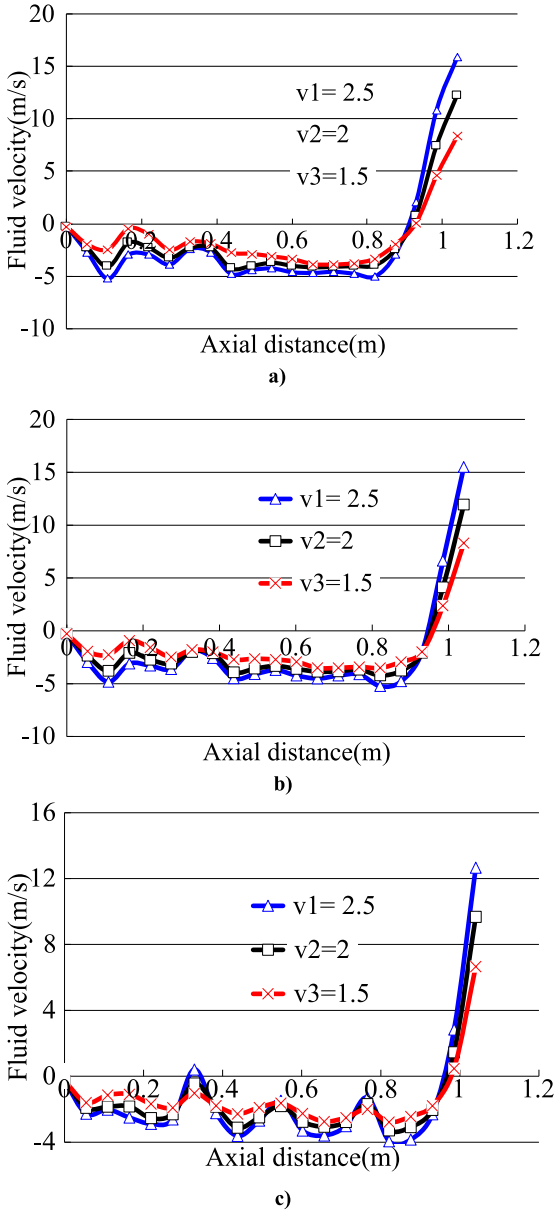


**FIGURE 13.** Distribution of fluid velocity in the radial direction around the leeward side of the rotor excitation winding. a) Sample line A. b) Sample line B. c) Sample line C.

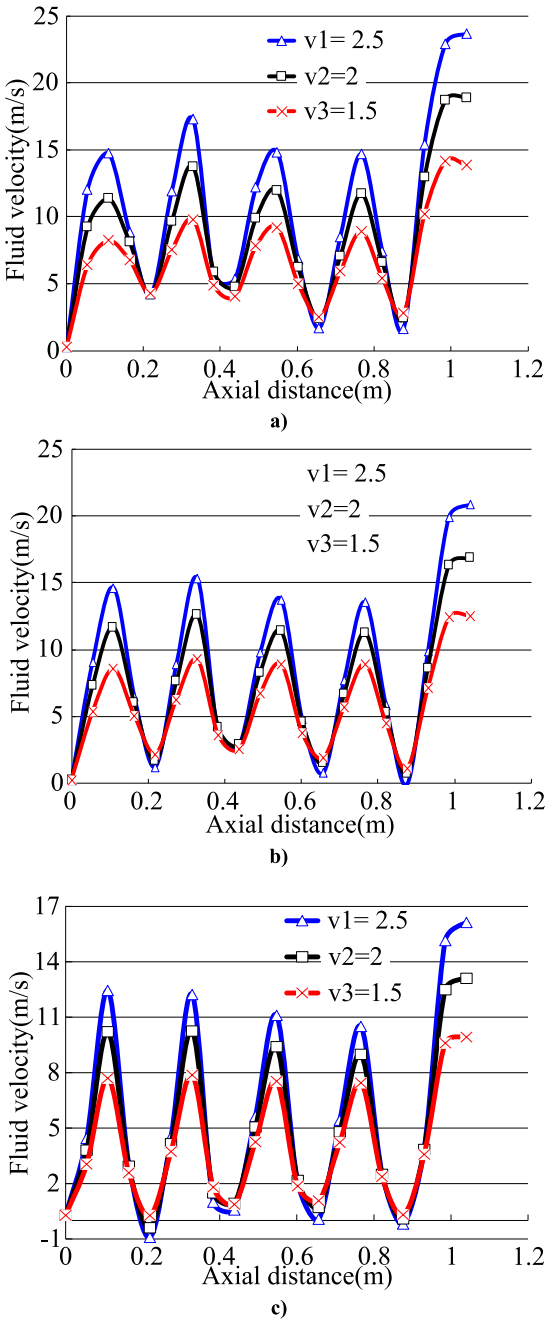


**FIGURE 14.** Distribution of fluid velocity in the radial direction around the windward side of the rotor excitation winding. a) Sample line D. b) Sample line E. c) Sample line F.

direction appears at the outlet of the rotor ventilation duct within the range of 0∼0.93m along the axial direction. The fluid velocity in the radial direction is still high in the rotor end region. There is an obvious difference in the distribution of fluid velocity in the radial direction around the windward side and the leeward side of the rotor excitation winding. The fluid velocity in the radial direction exists a wide range of negative values, which indicates that there is a backflow phenomenon between the rotor magnetic poles.

Fig. 15 and Fig. 16 show the distribution of fluid velocity in the axial direction around the leeward side and windward side of the rotor excitation winding. The fluid velocity in the axial direction is small. The highest fluid velocity around the windward side is 9m/s and the highest fluid velocity around the leeward side is 7.6m/s under the different fluid velocities of rotor region inlet. The fluid velocity in the axial direction is relatively high in the rotor end region.

It can be seen from Fig. 9-Fig. 16 that the change of the fluid velocity between the rotor magnetic poles affects directly the temperature distribution of the rotor excitation winding as the fluid velocity of the rotor region inlet increases. The average values of the synthetic fluid velocity,

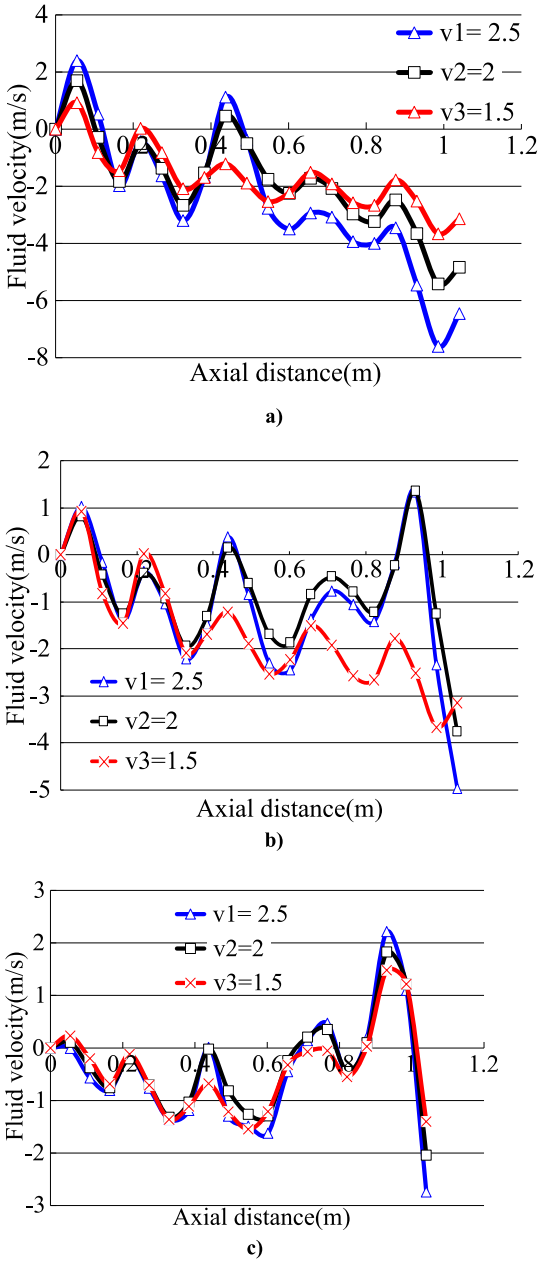


**FIGURE 15.** Distribution of fluid velocity in the axial direction around the leeward side of the rotor excitation winding. a) Sample line A. b) Sample line B. c) Sample line C.

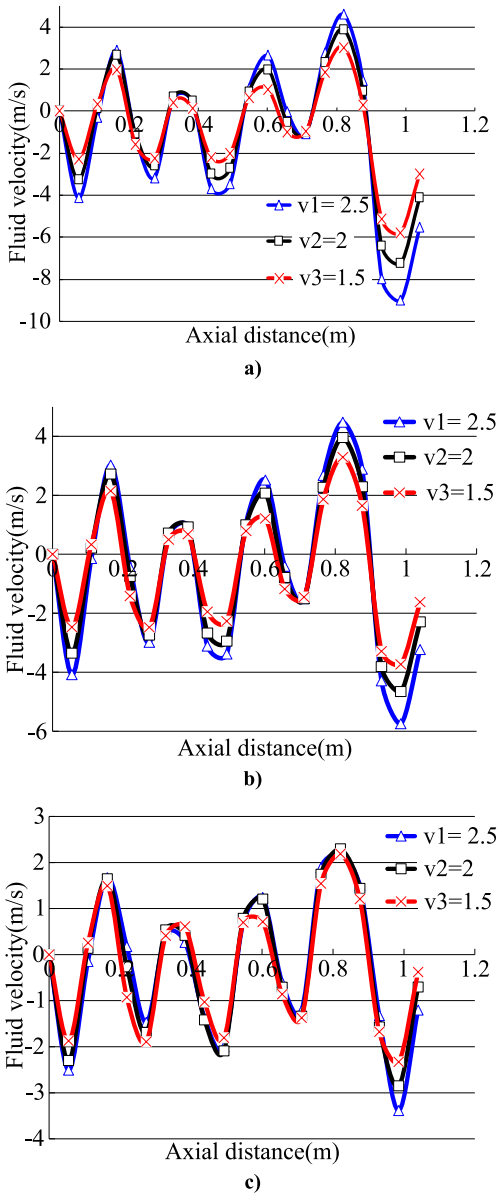


**FIGURE 16.** Distribution of fluid velocity in the axial direction around the windward side of the rotor excitation winding. a) Sample line D. b) Sample line E. c) Sample line F.

fluid velocity in the circumferential direction, fluid velocity in the radial direction, and fluid velocity in the axial direction are compared under the different flow rates, as shown in Table 3. It can be seen from Table 3 that the fluid velocity in the circumferential direction accounts for a large proportion of the synthetic fluid velocity around the leeward side and windward side of the rotor excitation winding. The fluid velocity in the circumferential direction remains basically unchanged as the fluid velocity of the rotor region inlet increases. It plays a major role in the cooling of the rotor excitation winding. The fluid velocity in the radial direction is relatively high around the windward side, which cannot be ignored in the cooling of rotor excitation winding. The fluid velocity in the axial direction has little effect on the cooling of rotor excitation winding. The fluid velocity in the radial direction and axial direction accounts for a small proportion of the synthetic fluid velocity around the leeward side and windward side of the rotor excitation winding.

### *B. TEMPERATURE DISTRIBUTION OF ROTOR COMPONENTS AND EXPERIMENTAL MEASUREMENT*

Fig. 17 shows the temperature distribution of rotor pole body, rotor press plate, rotor damping bar, rotor pole shoe, and

**TABLE 3. Average values of the fluid velocity in the different directions under the different flow rates.**

| | Fluid velocity of inlet (m/s) | Average value of fluid velocity | | | |
|---|---|---|---|---|---|
| | | Synthetic (m/s) | Circumferential direction (m/s) | Radial direction (m/s) | Axial direction (m/s) |
| Windward side | 2.5 | 59.6 | -57 | 8.9 | -0.6 |
| | 2 | 58.9 | -57.1 | 7.6 | -0.5 |
| | 1.5 | 58.4 | -57.3 | 6.2 | -0.5 |
| Leeward side | 2.5 | 58.5 | -57.9 | -2 | -1 |
| | 2 | 58.2 | -57.8 | -1.9 | -0.8 |
| | 1.5 | 58 | -57.8 | -1.6 | -0.8 |

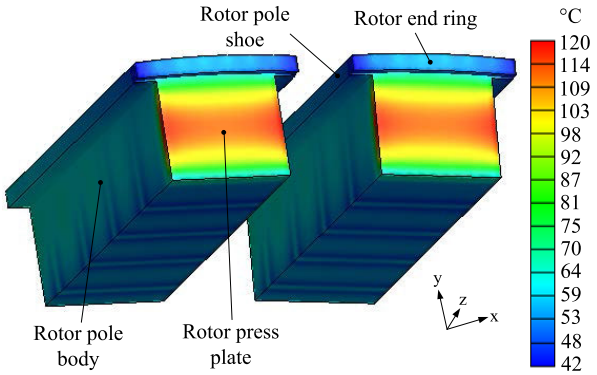


**FIGURE 17. Temperature distribution of rotor pole body, rotor press plate, rotor damping bar, rotor pole shoe, and rotor end ring.**

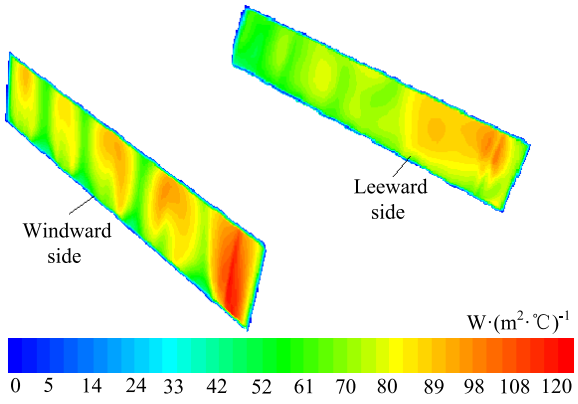


**FIGURE 18. Surface heat-transfer coefficient distribution of the rotor excitation winding.**

rotor end ring in the hydrogenerator rotor region. The highest temperature of these components appears in the rotor press plate and it is 120°C. The temperature of the rotor pole body is low around the outlet of the rotor radial ventilation duct. Fig. 18 shows the surface heat-transfer coefficient distribution of the rotor excitation winding when the fluid velocity of rotor region inlet is 2m/s. The maximum surface heat-transfer coefficient of the rotor excitation winding is 120 $W\cdot(m^2\cdot°C)^{-1}$. The surface heat-transfer coefficient distribution of the rotor excitation winding is uneven along the axial direction. Fig. 19 shows the temperature distribution

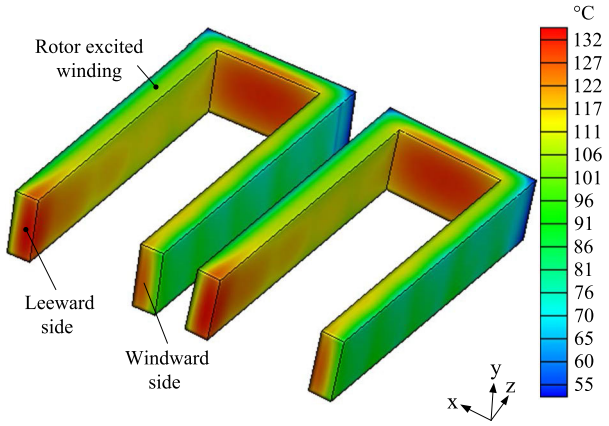


**FIGURE 19. Temperature distribution of the rotor excitation winding.**

**TABLE 4. Measured value and calculated result of the temperature of rotor excitation winding.**

| Rotor excitation winding | Measured value | Calculated result |
|---|---|---|
| Temperature (°C) | 108.6 | 106 |

of the rotor excitation winding when the fluid velocity of rotor region inlet is 2m/s. The highest temperature of the rotor excitation winding appears on the leeward side and it is 132°C. The average temperature of the rotor excitation winding is 106°C. The measured average temperature of the rotor excitation winding is 108.6°C. The measured value and calculated result of the temperature of rotor excitation winding are shown in Table 4. The calculated result is close to the measured value. It shows the calculated result is accuracy and the calculated method is reliable.

## V. CONCLUSION

In this paper, the influence of fluid velocity in the different directions on the temperature of the rotor excitation winding is studied under the different flow rates in the rotor region. The calculated temperature result agrees well with the measured value. Fluid velocity in the circumferential direction accounts for a large proportion of the synthetic fluid velocity around the leeward side and windward side of the rotor excitation winding. The fluid velocity in the circumferential direction remains basically unchanged as the fluid velocity of the rotor region inlet increases. It plays a major role in the cooling of the rotor excitation winding.

The fluid velocity in the radial direction is relatively high around the windward side, which cannot be ignored in the cooling of rotor excitation winding. The fluid velocity in the axial direction has little effect on the cooling of rotor excitation winding. The fluid velocity in the radial direction and axial direction accounts for a small proportion of the synthetic fluid velocity around the leeward side and windward side of the rotor excitation winding.

The highest temperature of rotor press plate is 120°C. The temperature of the rotor pole body is low around the outlet of the rotor radial ventilation duct. The maximum surface heat-transfer coefficient of the rotor excitation winding is 120 $W\cdot(m^2\cdot°C)^{-1}$. The surface heat-transfer coefficient distribution of the rotor excitation winding is uneven along the axial direction. The highest temperature of the rotor excitation winding appears on the leeward side of the rotor excitation winding and it is 132°C. The average temperature of the rotor excitation winding is 106°C.

## REFERENCES


[1] C. Carounagarane, T. R. Chelliah, and D. Khare, "Analysis on thermal behavior of large hydrogenerators operating with continuous overloads," *IEEE Trans. Ind. Appl.*, vol. 56, no. 2, pp. 1293–1305, Mar. 2020.

[2] H. C. Dirani, A. Merkhouf, B. Kedjar, A.-M. Giroux, and K. Al-Haddad, "Rotor interturn short circuit impact on large hydrogenerator magnetic quantities," *IEEE Trans. Ind. Appl.*, vol. 54, no. 4, pp. 3702–3711, Jul. 2018.

[3] G. Traxler-Samek, T. Lugand, and A. Schwery, "Additional losses in the damper winding of large hydrogenerators at open-circuit and load conditions," *IEEE Trans. Ind. Electron.*, vol. 57, no. 1, pp. 154–160, Jan. 2010.

[4] M. Ranlöf, R. Perers, and U. Lundin, "On permeance modeling of large hydrogenerators with application to voltage harmonics prediction," *IEEE Trans. Energy Convers.*, vol. 25, no. 4, pp. 1179–1186, Dec. 2010.

[5] A. Z. Gbégbé, B. Rouached, J. C. M. Bergeron, and P. Viarouge, "Damper currents simulation of large hydro-generator using the combination of FEM and coupled circuits models," *IEEE Trans. Energy Convers.*, vol. 32, no. 4, pp. 1273–1283, Dec. 2017.

[6] S. E. Dallas, A. N. Safacas, and J. C. Kappatou, "Interturn stator faults analysis of a 200-MVA hydrogenerator during transient operation using FEM," *IEEE Trans. Energy Convers.*, vol. 26, no. 4, pp. 1151–1160, Dec. 2011.

[7] J. C. Akiror, A. Merkhouf, C. Hudon, and P. Pillay, "Consideration of design and operation on rotational flux density distributions in hydrogenerator stators," *IEEE Trans. Energy Convers.*, vol. 30, no. 4, pp. 1585–1594, Dec. 2015.

[8] T. Øyvang, J. K. Nøland, G. J. Hegglid, and B. Lie, "Online model-based thermal prediction for flexible control of an air-cooled hydrogenerator," *IEEE Trans. Ind. Electron.*, vol. 66, no. 8, pp. 6311–6320, Aug. 2019.

[9] S. Li, C. Gong, N. A. Gallandat, J. R. Mayor, and R. G. Harley, "Implementation of surface impedance boundary conditions in the quasi three-dimensional finite-difference simulations of generator end regions," in *Proc. IEEE Int. Electr. Mach. Drives Conf. (IEMDC)*, May 2017, pp. 1–7.

[10] S. Li, C. Gong, N. A. Gallandat, J. R. Mayor, and R. G. Harley, "Analyzing the impact of press plate structure on the flux and loss distributions in the end region of large generators by transient 3-dimensional finite-element method with an improved core loss model," in *Proc. IEEE Int. Electr. Mach. Drives Conf. (IEMDC)*, May 2017, pp. 1–8.

[11] S. Li, C. Gong, L. Du, J. R. Mayor, R. G. Harley, and T. G. Habetler, "Fast calculation of the magnetic field and loss distributions in the stator core end packets and finger plates of large synchronous generators," in *Proc. IEEE Energy Convers. Congr. Expo. (ECCE)*, Sep. 2018, pp. 822–828.

[12] S. Li, C. Gong, J. R. Mayor, R. G. Harley, and T. G. Habetler, "Efficient calculation of the strand eddy current loss distributions in the end stepped-stator region of large synchronous generators," in *Proc. IEEE Energy Convers. Congr. Expo. (ECCE)*, Sep. 2018, pp. 1783–1789.

[13] S. Li, C. Gong, L. Du, J. R. Mayor, R. G. Harley, and T. G. Habetler, "Parametric study for the design of the end region of large synchronous generators based on three-dimensional transient finite element analysis," in *Proc. IEEE Energy Convers. Congr. Expo. (ECCE)*, Sep. 2018, pp. 7356–7362.

[14] S. D. Milic, A. D. Zigic, and M. M. Ponjavic, "Online temperature monitoring, fault detection, and a novel heat run test of a water-cooled rotor of a hydrogenerator," *IEEE Trans. Energy Convers.*, vol. 28, no. 3, pp. 698–706, Sep. 2013.

[15] M. Istad, M. Runde, and A. Nysveen, "A review of results from thermal cycling tests of hydrogenerator stator windings," *IEEE Trans. Energy Convers.*, vol. 26, no. 3, pp. 890–903, Sep. 2011.

[16] H. Jichao, L. Yufei, D. Jiechen, S. Yutian, G. Baojun, and L. Weili, "Thermal modeling and experimental validation in the rotor region of hydrogenerator with different rotor structures," *IEEE Access*, vol. 9, pp. 120001–120009, 2021.

[17] W. Li, X. Zhang, S. Cheng, and J. Cao, "Thermal optimization for a HSPMG used for distributed generation systems," *IEEE Trans. Ind. Electron.*, vol. 60, no. 2, pp. 474–482, Feb. 2013.

[18] S. Utegenova, F. Dubas, M. Jamot, R. Glises, B. Truffart, D. Mariotto, P. Lagonotte, and P. Desevaux, "An investigation into the coupling of magnetic and thermal analysis for a wound-rotor synchronous machine," *IEEE Trans. Ind. Electron.*, vol. 65, no. 4, pp. 3406–3416, Apr. 2018.

[19] J. Han, P. Zheng, Y. Sun, B. Ge, and W. Li, "Influence of electric shield materials on temperature distribution in the end region of a large water–hydrogen–hydrogen-cooled turbogenerator," *IEEE Trans. Ind. Electron.*, vol. 67, no. 5, pp. 3431–3441, May 2020.

[20] V. Madonna, P. Giangrande, G. Migliazza, G. Buticchi, and M. Galea, "A time-saving approach for the thermal lifetime evaluation of low-voltage electrical machines," *IEEE Trans. Ind. Electron.*, vol. 67, no. 11, pp. 9195–9205, Nov. 2020.

[21] T. D. Kefalas and A. G. Kladas, "Thermal investigation of permanent-magnet synchronous motor for aerospace applications," *IEEE Trans. Ind. Electron.*, vol. 61, no. 8, pp. 4404–4411, Aug. 2014.

[22] C. Sciascera, P. Giangrande, L. Papini, C. Gerada, and M. Galea, "Analytical thermal model for fast stator winding temperature prediction," *IEEE Trans. Ind. Electron.*, vol. 64, no. 8, pp. 6116–6126, Aug. 2017.

[23] J. Han, B. Ge, D. Tao, and W. Li, "Calculation of temperature distribution in end region of large turbogenerator under different cooling mediums," *IEEE Trans. Ind. Electron.*, vol. 65, no. 2, pp. 1178–1186, Feb. 2018.

[24] H. Vansompel, A. Yarantseva, P. Sergeant, and G. Crevecoeur, "An inverse thermal modeling approach for thermal parameter and loss identification in an axial flux permanent magnet machine," *IEEE Trans. Ind. Electron.*, vol. 66, no. 3, pp. 1727–1735, Mar. 2019.

[25] J. Han, B. Ge, and W. Li, "Influence of magnetic permeability of the press plate on the loss and temperature of the end part in the end region of a turbogenerator," *IEEE Trans. Ind. Electron.*, vol. 66, no. 1, pp. 162–171, Jan. 2019.

[26] N. Z. Popov and S. N. Vukosavic, "Estimator of the rotor temperature of induction machine based on terminal voltages and currents," *IEEE Trans. Energy Convers.*, vol. 32, no. 1, pp. 155–163, Mar. 2017.

[27] P. S. Nasab, R. Perini, A. Di Gerlando, G. M. Foglia, and M. Moallem, "Analytical thermal model of natural-convection cooling in axial flux machines," *IEEE Trans. Ind. Electron.*, vol. 67, no. 4, pp. 2711–2721, Apr. 2020.


**HAN JICHAO** was born in Harbin, China, in 1986. He received the B.S., M.S., and Ph.D. degrees in electrical machinery and appliance from the Harbin University of Science and Technology, Harbin, China, in 2010, 2013, and 2015, respectively. He is currently an Associate Professor with the Harbin University of Science and Technology. He is the author or coauthor of more than 20 refereed technical papers in IEEE TRANSACTIONS and IET proceedings, and he holds more than 20 invention patents. His research interests include research on ventilation cooling, electromagnetics, fluids, and thermal analysis on large electrical generators, particularly in large generator.

**SUN YUTIAN** was born in 1963. He received the B.S. and M.S. degrees in electrical machinery and appliance from the Harbin University of Science and Technology, Harbin, China, in 1984 and 1987, respectively, and the Ph.D. degree in electrical machine from the Shenyang University of Technology, Shenyang, in 1998. He is currently a Deputy Chief Designer with the State Key Laboratory of Hydro-Power Equipment, Harbin Electric Machinery Company Ltd., and the Harbin Institute of Large Electrical Machinery. He is engaged in the design of large generator.

**ZHENG PING** was born in 1969. She received the B.S., M.S., and Ph.D. degrees in electrical engineering from the Harbin Institute of Technology, Harbin, China, in 1992, 1995, and 1999, respectively. Since 1995, she has been with the Harbin Institute of Technology, where she has been a Professor, since 2005. She has authored or coauthored more than 270 published refereed technical papers and four books. She is the holder of 56 Chinese invention patents. Her current research interests include electric machines and control, hybrid electric vehicles, and unconventional electromagnetic devices.

**QI HAIMING** was born in Harbin, China, in 1997. He received the B.S. degree in electrical engineering and automation from the Harbin University of Science and Technology, Harbin, China, in 2021, where he is currently pursuing the M.S. degree in electrical machinery and appliance. His research interests include research on electromagnetics and thermal analysis on electrical generator.

**DONG JIECHEN** was born in Anda, China, in 1997. He received the B.S. degree in electrical engineering and automation from the Harbin University of Science and Technology, Harbin, China, in 2020, where he is currently pursuing the M.S. degree in electrical machinery and appliance. His research interests include research on ventilation cooling, fluids, and thermal analysis on electrical generator.

**LIU YUFEI** was born in Harbin, China, in 1997. He received the B.S. degree in electrical engineering and automation from the Harbin University of Science and Technology, Harbin, China, in 2019, where he is currently pursuing the M.S. degree in electrical machinery and appliance. His research interests include research on electromagnetics and thermal analysis on electrical generator.

**ZHANG CHUNLI** was born in 1975. He received the M.S. degree in electrical engineering from the Harbin Institute of Technology, Harbin, China, in 1997. He is currently a Senior Engineer with the Harbin Institute of Large Electrical Machinery. He is engaged in the electromagnetic analysis of large generator.

**GE BAOJUN** was born in 1960. He received the B.S. and M.S. degrees in electrical machinery and appliance from the Harbin University of Science and Technology, Harbin, China, in 1982 and 1985, respectively, and the Ph.D. degree in electrical machine and appliance from the Harbin Institute of Technology, Harbin, in 1999.

He is currently a Professor with the Harbin University of Science and Technology. He is also the Head of the National High Quality Courses of Electrical Machinery. He is the author or coauthor of more than 100 published refereed technical papers and four books. His research interests include new technology of large generator, electromechanical energy conversion, and coordinate theory of generators and power grids.

**LI WEILI** received the M.S. degree from the Harbin Institute of Electrical Technology, Harbin, China, in 1993, and the Ph.D. degree from the Russia Electric Power Research Institute, Saint Petersburg, Russia, in 1997.

He is currently a Professor with the Harbin University of Science and Technology. He is the author or coauthor of more than 200 published refereed technical papers and is the holder of 22 patents. His research interests include synthesis physical field analyses on large electrical machines, renewable energy systems, and special electrical machines and associated control.